

Improved random batch Ewald method in molecular dynamics simulations

Jiuyang Liang¹, Zhenli Xu^{*1,2}, and Yue Zhao¹

¹School of Mathematical Sciences, Shanghai Jiao Tong University, Shanghai, 200240, P. R. China

²Institute of Natural Sciences and MOE-LSC, Shanghai Jiao Tong University, Shanghai, 200240, P. R. China

April 29, 2022

Abstract

The random batch Ewald (RBE) is an efficient and accurate method for molecular dynamics (MD) simulations of physical systems at the nano-/micro- scale. The method shows great potential to solve the computational bottleneck of long-range interactions, motivating a necessity to accelerating short-range components of the non-bonded interactions for a further speedup of MD simulations. In this work, we present an improved RBE method for the non-bonding interactions by introducing the random batch idea to constructing neighbor lists for the treatment of both the short-range part of the Ewald splitting and the Lennard-Jones potential. The efficiency of the novel neighbor list algorithm owes to the stochastic minibatch strategy which can significantly reduce the total number of neighbors. We implement the improved RBE method in the LAMMPS package. The accuracy and stability of the algorithm are demonstrated by both theoretical analysis and benchmark simulations. Numerical tests on computer performance by conducting large-scaled MD simulations for systems including up to 0.1 billion water molecules, run on massive cluster with up to 50 thousand CPU cores, demonstrating the attractive features such as the high parallel scalability and memory-saving of the method in comparison to the existing methods.

Key words. Molecular dynamics simulations, electrostatics, random batch Ewald, random batch list

1 Introduction

Molecular dynamics (MD) furnishes a powerful tool for understanding equilibrium and dynamical properties of a broad range of systems at the molecular and atomic level [1, 2, 3, 4, 5], including physical, chemical, biological and materials sciences. To obtain the trajectories of particles by solving the equations of motion, one essential element for an MD simulation is a knowledge of the inter-particle potential from which the force acting on each particle can be calculated. The interaction force may vary from intramolecular forces to more complicated many-body forces between atoms and molecules, dominating the central processing unit (CPU) cost in comparison with other computational procedures such as thermostat and barostat. Once the interaction force can be successfully calculated, the equations of motion by Newton’s law are integrated to obtain the spatial position and temporal velocity of each atom at each time step.

Classical MD uses a molecular mechanics force field to model the inter-particle forces, which is a parameter set by fitting results of quantum mechanical calculations and, typically, to certain experimental measurements. Generally, the force field model [6] is composed of

*xuzl@sjtu.edu.cn

bond stretching, bending and torsional forces, and two non-bonded interactions including the van der Waals and electrostatic forces. From computational point of view, the bonded interactions are less expensive as the involving atoms are no more than three covalent bonds. Whereas, the non-bonded forces are the computational bottleneck as the electrostatic forces must be calculated between all pairs of particles, and the van der Waals forces need to calculate the pair interactions less than some cutoff radius ($0.9 \sim 1.5nm$), remaining a broad interest for algorithm development and optimization. Particularly, electrostatic interactions are ubiquitous in biomolecular and material systems such as DNA aggregation [7], protein folding/unfolding [8, 9, 10], the form of surface pattern [11], ion adsorption [12], and poly-electrolyte complexation [13]. An efficient and accurate electrostatic solver plays essential role for the simulations of these systems.

Various fast methods have been developed for the non-bonded interactions. It is noted that the Lennard-Jones (LJ) model is often used for the van der Waals force and it can be calculated with $\mathcal{O}(N)$ complexity due to the cutoff scheme [14] which truncates the interaction potential between a pair of particles at a radial cutoff distance and ignores the pairs of larger distances. Techniques such as the Verlet list method [15] and the linked cell list method [16] are often employed. In mainstream MD packages [17, 18], electrostatic interactions are calculated by the Ewald-type lattice summation where the long-ranged smooth part is treated on uniform mesh via fast Fourier transform [19, 20, 21] (FFT) with $\mathcal{O}(N \log N)$ complexity. The remaining part is short ranged and can be calculated by the cutoff scheme similar to the LJ interactions. It is mentioned that there are other kinds of powerful and linear-scaling method for fast evaluating electrostatic interactions, including fast multipole methods [22, 23], multigrids and Maxwell-equation molecular dynamics [24], where the fast multipole methods are particularly efficient for systems for large scale problems and for the case of inhomogeneous particle distribution [25, 26]. These fundamental methods for computing forces are all required to combine with modern distributed architectures, i.e., the well-known 3D domain decomposition [14, 27, 28]. The advances on domain decomposition, building neighbor lists, and time integration are contributed to the latest topics of algorithm development.

The calculation of long-ranged electrostatic interactions require intensive communications between cores, which significantly reduce the parallel efficiency for large scale systems [5, 29, 30, 31]. Besides, the proportion of the CPU cost on short-range interactions also tends to play an essential contribution due to the balance strategy [17, 18] between short-range and long-range interactions. A crucial observation [32, 33] is that there are decreasing marginal returns to algorithmic innovation, because the easy-to-catch innovations have already been “fished-out” [34] and the remaining is more difficult to find or provides smaller gains. For MD simulations, this marginal effect also arises, where the bottleneck on communication latency for the calculation of non-bonding forces has no transformative advances for several decades [29, 35].

In recent years, stochastic algorithms emerge gradually and furnish an important bridge linking traditional methods and modern massive high-performance computing, lifting both efficiency and scalability [36, 37]. For electrostatic interactions, the random batch Ewald (RBE) method proposed recently [38, 36], has presented its tremendous potential to overcome the scalability issues for deterministic algorithms such as particle-mesh Ewald. The RBE method is based on the Ewald summation. It avoids the use of the FFT by employing a random mini-batch importance sampling strategy on the Fourier components to approximate the force and pressure contributions from the long-range part. Since its superior speedup in the Fourier space, it is pointed out [36, 39] that the short-range part becomes the bottleneck of the MD simulations, and a further acceleration requires a high-efficient treatment of the short-range contributions of the non-bonded force, including the LJ and the real part of the Ewald splitting. For this purpose, in this paper we propose an improved RBE (IRBE) method employing the random batch list (RBL) scheme [40] to accelerate the short-range calculation under the RBE framework. Basically, the RBL does the random batch in the real space, resulting in a significant reduction in the number of neighbors for each particle. The RBL is an extension of the original random batch method [41] by dividing the region into a core-shell structure and constructing the minibatch for particles in the shell

region. This idea works well for the LJ potential [40], and in this paper we demonstrate its further extension in the IRBE method for a united scheme of the non-bonded interactions is effective. We present the accuracy and stability analysis of the IRBE method. The method is implemented in the LAMMPS package, and our numerical results demonstrate the attractive performance of the IRBE method by testing the accuracy and parallel efficiency for benchmark problems, showing its great promise in saving computer resources of both CPU and memory costs, thus furnishing a useful tool to address the above-mentioned marginal effect.

The rest of this paper is organized as follows. In Section 2, we briefly review the classical methods including the Ewald method and neighbor list method, and then describe the improved RBE method and theoretical analysis. The accuracy and performance tests of the resulting method are performed in Section 4. Conclusion and remarks are given in Section 5.

2 Methods

2.1 Classical non-bonded algorithms

Before presenting the IRBE method, we briefly review classical methods for evaluating non-bonded interactions in a 3D periodic system, including the Ewald and neighbor list methods.

Consider a system of N atoms with charge q_i at position \mathbf{r}_i for $i = 1, \dots, N$. These atoms are within a cubic simulation box Ω with side length L and volume $V = L^3$, with a periodic boundary condition specified to mimic a bulk environment. The charges in the system obey the neutrality condition $\sum_j q_j = 0$. Under these conditions, the non-bonded potential energy due to the LJ and electrostatic interactions can be written as the following lattice summation,

$$U = \frac{1}{2} \sum_{\mathbf{n}}' \sum_{i,j=1}^N \left\{ q_i q_j \frac{1}{|\mathbf{r}_{ij} + \mathbf{n}L|} + 4\epsilon_{ij} \left[\left(\frac{\sigma_{ij}}{|\mathbf{r}_{ij} + \mathbf{n}L|} \right)^{12} - \left(\frac{\sigma_{ij}}{|\mathbf{r}_{ij} + \mathbf{n}L|} \right)^6 \right] \right\}, \quad (2.1)$$

where $\mathbf{r}_{ij} := \mathbf{r}_j - \mathbf{r}_i$, \mathbf{n} runs over all 3D vector with integer components, and ϵ_{ij} and σ_{ij} are the depth of the LJ potential well and the distance where the potential changes sign between i th and j th particles, respectively. The prime in Eq.(2.1) is understood that the singular term when $i = j$ and $\mathbf{n} = (0, 0, 0)$ should be excluded. The difficulties of calculating Eq.(2.1) is twofold. First, the long-range nature of the Coulomb potential leads to the conditionally convergent series, thus the direct truncation will produce artifacts[14] and should be avoided. Second, the short-range part requires expensive $\mathcal{O}(N^2)$ cost for directly searching neighbors within a given radius at each time step.

Ewald summation[42] addresses the first problem by a splitting strategy which decomposes the Coulomb kernel into a sum of two components,

$$\frac{1}{r} = \frac{\text{erf}(\sqrt{\alpha}r)}{r} + \frac{\text{erfc}(\sqrt{\alpha}r)}{r}. \quad (2.2)$$

Here α is a positive parameter controlling the decay rate of real space and Fourier space series, $\text{erf}(x) := (2/\sqrt{\pi}) \int_0^x e^{-u^2} du$ is the error function, and $\text{erfc}(x) = 1 - \text{erf}(x)$ denotes the error complementary function. After the Ewald splitting, the first component in Eq.(2.2) becomes long ranged and smooth, thus can be handled in the Fourier space via the so-called Fourier transform, $\hat{f}(\mathbf{k}) = \int_{\Omega} f(\mathbf{r}) e^{-i\mathbf{k} \cdot \mathbf{r}} d\mathbf{r}$, where $\mathbf{k} = 2\pi\mathbf{m}/L$ with $\mathbf{m} \in \mathbb{Z}^3$. The second component in Eq.(2.2) is singular but short ranged, and thus can be truncated at a certain cutoff radii r_c . Denote k_c and r_{lj} as the cutoff of the Fourier space and the cutoff of the LJ potential, respectively. The non-bonded potential energy U by Eq.(2.1) can be rewritten as

a sum of the following four contributions:

$$\begin{aligned}
U^{short} &= \frac{1}{2} \sum_{|\mathbf{r}_{ij} + \mathbf{n}L| \leq r_c} q_i q_j \frac{\text{erfc}(\sqrt{\alpha}|\mathbf{r}_{ij} + \mathbf{n}L|)}{|\mathbf{r}_{ij} + \mathbf{n}L|}, \\
U^{lj} &= \frac{1}{2} \sum_{|\mathbf{r}_{ij} + \mathbf{n}L| \leq r_{lj}} 4\epsilon_{ij} \left[\left(\frac{\sigma_{ij}}{|\mathbf{r}_{ij} + \mathbf{n}L|} \right)^{12} - \left(\frac{\sigma_{ij}}{|\mathbf{r}_{ij} + \mathbf{n}L|} \right)^6 \right], \\
U^{long} &= \frac{2\pi}{V} \sum_{\substack{\mathbf{k} \neq \mathbf{0} \\ |\mathbf{k}| \leq k_c}} \frac{1}{|\mathbf{k}|^2} |\rho(\mathbf{k})|^2 e^{-|\mathbf{k}|^2/4\alpha}, \\
U^{corr} &= -\sqrt{\frac{\alpha}{\pi}} \sum_{i=1}^N q_i^2,
\end{aligned} \tag{2.3}$$

where U^{short} and U^{long} are short- and long-range parts of the electrostatic interactions, U^{lj} is the LJ interaction, and U^{corr} is the correction term due to the self energy. The structure factor $\rho(\mathbf{k})$ is the conjugate of the Fourier transform of the charge density, defined as

$$\rho(\mathbf{k}) := \sum_{i=1}^N q_i e^{i\mathbf{k} \cdot \mathbf{r}_i}. \tag{2.4}$$

By proper choice of the parameters (α and the real-space and Fourier-space cutoffs r_c and k_c), the computational complexity for both U^{long} and U^{short} is optimized to $\mathcal{O}(N^{3/2})$ [43, 14]. Moreover, the FFT is often employed to further speed up the evaluation of U^{long} such that the cutoff radius r_c can be much smaller, resulting in the core algorithms for mainstream software, including the particle-particle particle-mesh Ewald [20] (PPPM), particle mesh Ewald [19], and smooth particle mesh Ewald [21] algorithms. The final computational complexity of $\mathcal{O}(N \log N)$ can be achieved through these methods for periodic systems.

With the FFT acceleration on U^{long} , the cutoff radius r_c is often set to be the same as r_{lj} so that U^{short} and U^{lj} can use the same neighbor list. Then, to handle the short-range part efficiently, a Verlet-style neighbor list [15] is often created. This neighbor list enumerates all pairs of atoms with separation less than a cutoff distance. The building of neighbor list involves a stencil of bins to check for possible neighbors, a procedure for binning atoms, and a loop on the resulting stencil to assemble the neighbor list according to some cutoff criterions. The Verlet list [15] also introduces an additional larger cutoff radius to reduce the frequency of neighbor list establishment. Building such a local neighbor list is in linear time, and the complexity of evaluating $U^{short} + U^{lj}$ also achieves linear scaling. The prefactor is related to both the cutoff radii and the bin size. A significant problem of classical neighbor list method is that the neighbor list typically consume the most memory of any data structure in the mainstream MD software [17, 18]. This is mainly because the average number of particles within the cutoff radius can be large for heterogeneous systems due to the use of a big radius. As an example, the bulk water system is often simulated with cutoff radius $r_c = 1.2nm$ with which the average number of neighbors is ~ 700 .

A lot of techniques have been developed to optimize the Verlet list method, aiming at the reduction in both the memory access and computational cost. Many of them are devoted to the improvement of the linked cell list method [44, 45] employed for the Verlet list construction. There are also attempts on providing scalable algorithms that work well on a modern computer architecture, including multi-core CPU, graphics processing unit, or even more in-depth coding technologies such as the single-instruction multiple data (SIMD) vectorization instructions [46, 47, 17, 48].

Finally, the atomic non-bonded force is obtained as the negative gradient of the energy

function U , which is given by,

$$\begin{aligned}\mathbf{F}_i^{short} &= -q_i \sum_{r_{ij} \leq r_c} ' q_j \left[\frac{\text{erfc}(\sqrt{\alpha} r_{ij})}{r_{ij}^2} + \frac{2\sqrt{\alpha} e^{-\alpha r_{ij}^2}}{\sqrt{\pi} r_{ij}} \right] \frac{\mathbf{r}_{ij}}{r_{ij}}, \\ \mathbf{F}_i^{lj} &= - \sum_{r_{ij} \leq r_c} ' \epsilon_{ij} \left(\frac{48\sigma_{ij}^{12}}{r_{ij}^{14}} - \frac{24\sigma_{ij}^6}{r_{ij}^8} \right) \mathbf{r}_{ij}, \\ \mathbf{F}_i^{long} &= - \sum_{\mathbf{k} \neq \mathbf{0}} \frac{4\pi q_i \mathbf{k}}{V |\mathbf{k}|^2} e^{-|\mathbf{k}|^2/4\alpha} \text{Im}(e^{-i\mathbf{k} \cdot \mathbf{r}_i} \rho(\mathbf{k})),\end{aligned}\tag{2.5}$$

where $r_{ij} = |\mathbf{r}_{ij}|$, and j runs over all particles in the central box and periodic images. It is noted that \mathbf{F}_i^{short} and \mathbf{F}_i^{lj} are singular but short-range, and \mathbf{F}_i^{long} is smooth and long-range, corresponding to the terms in Eq.(2.3). The correction term in (2.3) is constant for given α and makes no contribution to the force.

As was pointed out[49, 48], the enormous memory consumption of neighbor list for evaluating short-range interactions and the intensive communication of FFT for evaluating long-range interactions are two bottlenecks of MD simulations, limiting both the system scale and the time scale. In the next section, we attempt to address these bottlenecks by developing the IRBE method.

2.2 Random batch importance sampling

The RBE is a fast algorithm for calculating the long-range force \mathbf{F}_i^{long} . Its idea is based on an observation that the Gaussian factor $e^{-|\mathbf{k}|^2/4\alpha}$ in Eq.(2.5) can be normalized as a discrete probability distribution[38]. Consider the following identity,

$$S := \sum_{\mathbf{k} \neq \mathbf{0}} e^{-\mathbf{k}^2/(4\alpha)} = H^3 - 1,\tag{2.6}$$

where H can be represented as follows by the Poisson summation formula,

$$H := \sum_{m \in \mathbb{Z}} e^{-\pi^2 m^2 / (\alpha L^2)} = \sqrt{\frac{\alpha L^2}{\pi}} \sum_{m \in \mathbb{Z}} e^{-\alpha m^2 L^2}.\tag{2.7}$$

In our applications, $\alpha L^2 \gg 1$ holds and one can truncate m at ± 1 , resulting in an efficient approximation in the rightmost of Eq.(2.7). One can regard the series summation as a functional expectation over the probability distribution

$$\mathcal{P}_{\mathbf{k}} := S^{-1} e^{-|\mathbf{k}|^2/(4\alpha)}, \quad \mathbf{k} \neq \mathbf{0}.\tag{2.8}$$

Since the Gaussian distribution is separable in multiple dimensions, $\mathcal{P}_{\mathbf{k}}$ can be sampled independently in each axis with $\mathbf{k} = \mathbf{0}$ being skipped. For more details, one samples from 1D Gaussian distribution $x^* \sim \mathcal{N}(0, \alpha L^2 / (2\pi^2))$ and set $m^* = \text{round}(x^*)$, the acceptance rate is high via the Metropolis-Hasting sampling algorithm[14]. This procedure is independently repeated for three times. A highly efficient parallel strategy for the importance sampling under NVT/NPT ensemble is also developed[36]. The MD simulations can then be performed via the random mini-batch approach with this importance sampling strategy. Specially, one can approximate the long-range force \mathbf{F}_i^{long} in Eq.(2.5) by the following random variable

$$\mathbf{F}_i^{long,*} := - \sum_{\ell=1}^p \frac{S}{p} \frac{4\pi \mathbf{k}_{\ell} q_i}{V |\mathbf{k}_{\ell}|^2} \text{Im}(e^{-i\mathbf{k}_{\ell} \cdot \mathbf{r}_i} \rho(\mathbf{k}_{\ell})),\tag{2.9}$$

where \mathbf{k}_{ℓ} , $1 \leq \ell \leq p$, are the sampled frequencies. In the RBE method[38], the choice of parameter α shares the same strategy as in the PPPM method[50], such that the computational complexity for the short-range interactions is $\mathcal{O}(N)$. If we choose p as an $\mathcal{O}(1)$ constant, the complexity for approximating \mathbf{F}_i^{long} via Eq.(2.9) is also linear, namely, with complexity $\mathcal{O}(pN)$.

2.3 Improved RBE method

The RBE has shown its superscalability in large-scale all-atom simulations [36], resulting in that the evaluation of short-range non-bonded interactions becomes the most time-consuming part [39]. To reduce the calculation for short-range interactions and save CPU memory in the original RBE method, we introduce the RBL algorithm, first proposed for pure LJ fluid systems [40].

The RBL idea is based on a neighbor-splitting strategy. Let r_c be the cutoff radius for calculating both \mathbf{F}_i^{short} and \mathbf{F}_i^{lj} ; typically, $r_c = 1.2nm$ for all-atom simulations thus there are hundreds of neighbors for each particle should be stored in the neighbor list. The RBL method introduces the second radius $r_\eta < r_c$ (e.g., $r_\eta = 0.6nm$) such that two-level core-shell structured neighbor lists are constructed around each particle. Direct summation is used for neighbors within the core region ($r_{ij} < r_\eta$), whereas a small number of particles from the shell zone are randomly chosen into a batch and other neighbors in the zone are ignored. The central particle then interacts with the batch particles with a rescaled strength. This idea is demonstrated that the average interacting neighbors of each particle are significantly reduced, and the accuracy is maintained by resolving the kernel singularity issue for the LJ systems [40].

Let $\mathcal{F}_i = \mathbf{F}_i^{short} + \mathbf{F}_i^{lj}$ be the short-range non-bonded force on the i th particle. Let $\mathcal{C}(i) = \{j \neq i : r_{ij} \leq r_\eta\}$ and $\mathcal{S}(i) = \{j : r_\eta < r_{ij} \leq r_c\}$ be the neighbor sets of the i th particle in the core and shell regions, respectively. We now decompose it into the contributions from the core and the shell regions, separately, $\mathcal{F}_i = \mathcal{F}_i^{core} + \mathcal{F}_i^{shell}$, where $\mathcal{F}_i^{core} = \sum_{j \in \mathcal{C}(i)} \mathbf{f}_{ij}$, and $\mathcal{F}_i^{shell} = \sum_{j \in \mathcal{S}(i)} \mathbf{f}_{ij}$, and the force contribution due to particle j is,

$$\mathbf{f}_{ij} = -q_i q_j \left[\frac{\text{erfc}(\sqrt{\alpha} r_{ij})}{r_{ij}^2} + \frac{2\sqrt{\alpha} e^{-\alpha r_{ij}^2}}{\sqrt{\pi} r_{ij}} \right] \frac{\mathbf{r}_{ij}}{r_{ij}} - \epsilon_{ij} \left(\frac{48\sigma_{ij}^{12}}{r_{ij}^{14}} - \frac{24\sigma_{ij}^6}{r_{ij}^8} \right) \frac{\mathbf{r}_{ij}}{r_{ij}}. \quad (2.10)$$

Let $\mathcal{B}(i)$ be the batch of \tilde{p} particles randomly chosen from set $\mathcal{S}(i)$. By following the random batch method [41], the force \mathcal{F}_i^{shell} is approximated by

$$\mathcal{F}_i^{shell,*} = \frac{N_S}{\tilde{p}} \sum_{j \in \mathcal{B}(i)} \mathbf{f}_{ij}, \quad (2.11)$$

where N_S is the size of set $\mathcal{S}(i)$. It can be proved that the approximation is an unbiased estimate of the exact force from those particles in $\mathcal{S}(i)$. Let $\mathcal{F}^{corr} = \sum_i (\mathcal{F}_i^{core} + \mathcal{F}_i^{shell,*}) / N$ be the average net force on each particle, which is a random variable with zero expectation and bounded variance. One then obtains the stochastic approximation for short-range force, expressed by

$$\mathcal{F}_i \approx \mathcal{F}_i^{core} + \mathcal{F}_i^{shell,*} - \mathcal{F}^{corr}. \quad (2.12)$$

It is noted that the subtraction of the net force ensures the conservation of the total momentum in the system. We shall also remark that the random batch idea leads to a significant reduction of neighbors, as analyzed below.

Now by introducing the RBL for the real space to the RBE, we develop an integrated stochastic approximation of the non-bonded force, namely the IRBE method. The error estimate of this approximation is given in 2.4. We remark that we use two batch sizes \tilde{p} and p for the short-range force and the long-range force, respectively. These two sizes are determined by the specific systems and can be different. They are both $\mathcal{O}(1)$ constants. Another remark is that the IRBE method brings in an additional variance in the force term, leading to the numerical heating effect. Therefore, at the moment, this method is not suitable for long time simulations under the microcanonical ensembles, similar to the previous work [38, 40]. One shall develop an appropriate symplectic scheme for the time integration of the equations of motion, which remains an open problem for our stochastic algorithms. Fortunately, it is practical for the NVT and NPT ensembles with the use of thermostats and barostats.

In practice, to improve the efficiency, the simulation box is divided into uniform cells of edge r_η , and the particle list in each cell is built. For a given particle i , the core list is

Algorithm 1 (Improved random batch Ewald)

- 1: Input initial data: number of particles N , volume V , temperature T , simulation steps N_{tot} , and the initial particle information $\{\mathbf{r}_i, \mathbf{v}_i, q_i\}$. Choose parameters α , r_c , r_η , k_c , and batch sizes p and \tilde{p}
 - 2: Generate enough samples of $\mathbf{k} \sim e^{-|\mathbf{k}|^2/4\alpha}$ ($\mathbf{k} \neq 0$) by the Metropolis-Hastings procedure to form a sample set \mathcal{K}
 - 3: **for** n in $1 : N_{tot}$ **do**
 - 4: Divide the system into small cells of side length r_η , transmit particle information to different nodes, and create the core neighbor lists
 - 5: For each particle i , randomly choose \tilde{p} particles from its stencils if $N_S > \tilde{p}$, otherwise choose all particles
 - 6: Calculate short-range force \mathcal{F}_i^{core} with particles in the core region
 - 7: Calculate the stochastic force $\mathcal{F}_i^{shell,*}$ in the shell zone by Eq.(2.11) and the correction force
 - 8: Calculate the short-range forces $\mathcal{F}_i^* \approx \mathcal{F}_i^{core} + \mathcal{F}_i^{shell,*} - \mathcal{F}^{corr}$
 - 9: Choose p samples from set \mathcal{K} and calculate the long-range force $\mathbf{F}_i^{long,*}$ by Eq.(2.9)
 - 10: Calculate the total non-bonding force $\mathbf{F}_i^{tot,*} = \mathbf{F}_i^{long,*} + \mathcal{F}_i^*$
 - 11: Integrate Newton's equations with suitable integrate scheme and thermostat
 - 12: **end for**
-

constructed from the nearest 27 cells containing particles with distance less than r_η . Then, a stencil of cells, i.e., a combination of all neighboring particles of i into uniformly sized cells of width r_η , is used for constructing the shell list. In other words, the stencil is a larger cubic box comprised of $(2\lfloor r_c/r_\eta \rfloor + 3)^3$ cells where particle i is located at the central cell. It is feasible to apply the RBL method directly within this large stencil, avoiding the filter step for all particles. Then the core and shell neighbor sets are constructed and the corresponding forces \mathcal{F}_i^{core} and $\mathcal{F}_i^{shell,*}$ can be calculated, as mentioned in 2.3. Two things need to be remarked. First, in practice, the edge of the cell can be slightly larger than r_η so that updating the neighbor list is not required at every step[17]. Second, depending on the interatomic potentials, multiple neighbor lists and stencils with different attributes may be needed. One example is a solvated colloidal system with large colloidal particles where colloid/colloid, colloid/solvent, and solvent/solvent interaction cutoffs can be dramatically different[51, 47]. The procedure of the IRBE method is summarized in Algorithm 1.

It is stressed that the storage consumption and computational complexity of the RBL are all relatively small, in comparison to the classical direct truncation method with the Verlet list approach. Without loss of generality, suppose that the particles are uniformly distributed with ρ be the average particle density. The calculation complexity and the CPU memory usage for storing the neighbor list per particle in the classical method is $\mathcal{O}(4\pi r_c^3 \rho/3)$, whereas the RBL reduce these cost to $\mathcal{O}(4\pi r_\eta^3 \rho/3 + \tilde{p})$. If one safely adopts $r_c/r_\eta = 2.5$ and an appropriate \tilde{p} , both the storage saving and the speedup have about an order of magnitude improvement for the short-range interactions. Regarding the Fourier space, the computational complexity of the RBE method is only $\mathcal{O}(pN)$, where p is often chosen as a few hundred, and It avoids the multiple, massive global communications of the FFT calculation. These will be further discussed from numerical results in Section 3.

2.4 Error analysis

We conduct some analysis and discussions on the IRBE method to demonstrate its validity. Let \mathbf{F}_i^{tot} be the total non-bonded force on particle i , and $\mathbf{F}_i^{tot,*}$ is its approximation by the IRBE method. Let $\chi_i = \mathbf{F}_i^{tot} - \mathbf{F}_i^{tot,*}$ be the deviation of the approximate force. It is obvious by following the proof in literature [38, 40] that the expectation of χ_i is zero, i.e., $\mathbf{F}_i^{tot,*}$ is an unbiased estimator. The variance of the force approximation can be written as

$$\text{var}[\chi_i] = \text{var}[\mathcal{F}_i^*] + \text{var}[\mathbf{F}_i^{long,*}] \quad (2.13)$$

because the random mini-batches for approximating the short-range and the long-range force are mutually independent.

It is noted that the estimate of the long-range force has been obtained under the Debye-Hückel assumption [38],

$$\text{var}[\mathbf{F}_i^{\text{long},*}] \lesssim \frac{N^{4/3}}{pL^4}. \quad (2.14)$$

Combining this result, we have Theorem 2.1 for the estimate for the total force.

Theorem 2.1. *Under the assumption of the Debye-Hückel theory for particle distribution, the variance of the difference between approximated and exact non-bonded force holds the following estimate:*

$$\text{var}[\chi_i] \lesssim \frac{(N_S - \tilde{p})}{\tilde{p}} \rho \left[r_\eta^{-11} + \text{erfc}(\sqrt{2\alpha}r_\eta) \right] + \frac{N^{4/3}}{pL^4}. \quad (2.15)$$

Proof. By following the results given in Refs.[40, 38], the short-range part can be estimated by

$$\text{var}[\mathcal{F}_i^*] \lesssim \frac{N_S - \tilde{p}}{N^2 \tilde{p}} \left[\sum_{i \neq j} (N^2 - 2N) (\mathbf{f}_{ij})^2 + \sum_k \sum_{k \neq j} (\mathbf{f}_{ij})^2 \right], \quad (2.16)$$

where the minimum image conventions are already included in the force term [14]. The short-range force \mathbf{f}_{ij} is comprised of the short-range Ewald and the LJ forces. We consider these two parts separately, i.e., the variance of the short-range force is estimated by,

$$\text{var}[\mathcal{F}_i^*] \leq \text{var}[\mathbf{F}_i^{\text{short},*}] + \text{var}[\mathbf{F}_i^{\text{LJ},*}]. \quad (2.17)$$

We first consider the short-range Ewald force

$$\mathbf{f}_i^{\text{short}}(\mathbf{r}) = -q_i q_j \left[\frac{\text{erfc}(\sqrt{\alpha}r)}{r^2} + \frac{2\sqrt{\alpha}e^{-\alpha r^2}}{\sqrt{\pi}r} \right] \frac{\mathbf{r}}{r} \quad (2.18)$$

between particle q_i and q_j with the distance vector \mathbf{r} . When r is large, one has

$$\frac{\text{erfc}(\sqrt{\alpha}r)}{r^2} = \frac{2}{\sqrt{\pi}} \frac{\int_{\sqrt{\alpha}r}^{\infty} e^{-u^2} du}{r^2} \lesssim C \frac{e^{-\alpha r^2}}{r^3} = o\left(\frac{e^{-\alpha r^2}}{r}\right), \quad (2.19)$$

where C is constant depending on α . Thus the upper bound on the variance of the approximation of the short-range Ewald force can be derived by estimating the contribution from the second term in Eq.(2.18)

$$\text{var}[\mathbf{F}_i^{\text{short},*}] \lesssim \frac{(N_S - \tilde{p})}{\tilde{p}} \int_{r_\eta}^{\infty} 4\pi \rho r^2 \left| \frac{e^{-\alpha r^2}}{r} \right|^2 dr \lesssim \frac{(N_S - \tilde{p})}{\tilde{p}} \rho \text{erfc}(\sqrt{2\alpha}r_\eta). \quad (2.20)$$

Applying the same approach to the variance of the LJ force, one obtains

$$\text{var}[\mathbf{F}_i^{\text{LJ},*}] \lesssim \frac{(N_S - \tilde{p})}{\tilde{p}} \rho r_\eta^{-11}. \quad (2.21)$$

By combing Eqs.(2.17), (2.20), (2.21) with (2.14), we obtain (2.15) and complete the proof. \square

By Theorem 2.1, we can safely suppose that $\text{var}[\chi_i]$ is bounded by a constant ξ at the sense of infinite norm. Suppose that $\{\mathbf{r}_i, \mathbf{v}_i\}$ and $\{\mathbf{r}_i^*, \mathbf{v}_i^*\}$ are the configuration produced by the MD simulation using deterministic force and the IRBE, respectively. The following strong error holds,

$$\mathbb{E} \left[\frac{1}{N} \sum_i (|\mathbf{r}_i - \mathbf{r}_i^*|^2 + |\mathbf{v}_i - \mathbf{v}_i^*|^2) \right] \lesssim \sqrt{\xi \Delta t}, \quad (2.22)$$

where Δt is the time step. This can be proved by following the procedure similar to previous works [41, 40] through the Ito's formula in the discrete time interval. The convergence analysis indicates that our method is valid for capturing the finite time dynamics, and is demonstrated by the simulation results provided in the next section.

3 Results and discussion

In this section, we perform numerical results on two typical systems: primitive-model electrolyte solutions and all-atom bulk water systems at the NVT ensemble in order to validate the accuracy and efficiency of the proposed IRBE method. The results of two different methods are also performed for comparison. One is the PPPM method[52] which is a classical method for popular MD packages. The other is the RBE method which does not introduce the RBL for the short-range interactions. The calculations are conducted in the LAMMPS [27, 17] (version 29Oct2020) with the implementation of the RBE and IRBE, and on the “Siyuan Mark-I” cluster at Shanghai Jiao Tong University, which comprises 936 nodes with $2 \times$ Intel Xeon ICX Platinum 8358 CPU (2.6GHz, 32 cores) and 512 GB memory per node. Our implementation is optimized with distributed-memory parallelism via MPI and Intel 512-bit SIMD (AVX-512 architecture) instruction. The communication and vectorization procedures are described below in details.

A 3D domain decomposition strategy is coupled with for the calculation of real-space forces. The simulation box is spatially decomposed (partitioned) into non-overlapping sub-domains which fill the box. An unique MPI rank or process is assigned to each subdomain, such that the computational tasks assigned to each rank are even out as far as possible. The 3D decomposition framework is of great important in modern MD software and has been attracted many interests [17, 18, 46]. We follow the procedure described in Ref.[17] for the dynamic load-balanced partitioning and the ghost-atom communication, whereas the construction of neighbor lists uses the strategy provided in Section 2.3 of this paper.

For the long-range force, owing to the random batch idea in the Fourier space, a serial importance sampling procedure and a global broadcast operation seems to be required at each MD step. We note that this cost can be significantly reduced by using parallel sampling strategy[36]. The samples and the positions of particles are packaged into 512-bit vectors when the structure factors $\rho(\mathbf{k})$ are evaluated using the local atoms of each MPI rank. Only one global operation, MPI_Allreduce, is required for reducing $\rho(\mathbf{k})$. The approximated force $\mathbf{F}_i^{long,*}$ of each particle are then obtained from the structure factors.

3.1 Electrolyte solution

To demonstrate the performance of our approach, we first perform MD simulations of simple 1:1 and 2:1 electrolytes in the canonical ensemble. The electrolytes are described by the primitive model where ions are immersed in a continuum solvent and represented as soft spheres that interact via a shifted-truncated LJ potential and electrostatic interactions. The temperature is maintained by using a Langevin thermostat. The simulation proceeds with velocity-Verlet scheme. In each simulation, we perform 5×10^5 time steps for the equilibrium phase and 6×10^5 time steps for the statistics.

The system includes 2560 monovalent anions and 2560 monovalent cations in 1:1 electrolyte, while 1280 divalent cations and 2560 monovalent anions in 2:1 electrolyte, and all quantities are provided in reduced units. We fix the diameter of particles as $\sigma = 1$, and the side length of the simulation box is $L = 80\sigma$. The MD time step is set as $\tau = 0.002t_0$, where $t_0 = \sigma\sqrt{m_0/k_B T}$ is the unit of time with the particle mass $m_0 = 1$. The relaxation time is set to be $\gamma = 1.0$ for the Langevin thermostat.

We first examine the accuracy by calculating the radial distribution function (RDF) between ions of different species and the mean-square displacement (MSD) of different kinds of ions. The RDFs of atom pairs, denoted by g_{++} , g_{-+} and so on, furnish the spatial arrangement of the electrolyte system and the MSD shows uniform linear motion in short time and diffusion behavior in long time of particles. We use the PPPM method with 10^{-4} relative accuracy and cutoff $r_c = 15\sigma$ as the reference result. In the IRBE, we set $r_\eta = 5\sigma$ and batch size $\tilde{p} = 10$ for the short-range force, and $\alpha = 0.03$ (the same as for the PPPM) and batch size $p = 100$ (the same as for the RBE) for the long-range force. The results are displayed in Fig. 1, showing the three methods are almost overlapping in both the RDF and MSD curves, demonstrating that the IRBE reproduces both structural and dynamical properties of the RBE and PPPM methods. During the simulations, we compute

the average number of neighbors per atom. There are ~ 140 neighbors for both the PPPM and the RBE, whereas only ~ 10 of them are inside the core region, indicating that the IRBE significantly reduces the number of neighbors, and thus it will be promising to save the memory and CPU costs, as is shown later on. In Fig. 2, the potential energy per atom of every 100 time steps are plotted by using different methods. The mean and standard deviation value are listed in Table. 1. The relative errors of the IRBE method have minor differences in comparison with the PPPM and the RBE.

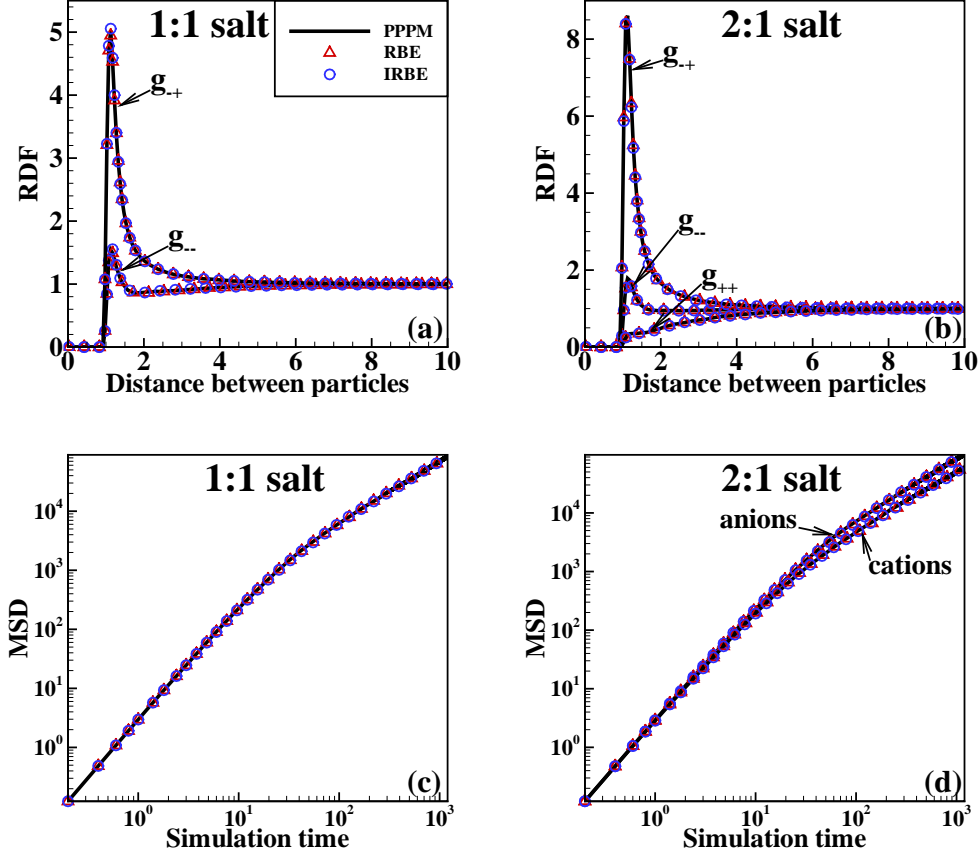


Figure 1: RDFs and MSDs of the 1:1 and 2:1 electrolytes calculated by three different methods.

Table 1: Mean value (mean) and standard deviation (std) of the potential energy per atom displayed in Figure 2.

	PPPM	RBE	IRBE
1 : 1 mean	-0.2544	-0.2559	-0.2538
1 : 1 std	0.005968	0.006289	0.005885
2 : 1 mean	-0.4505	-0.4516	-0.4467
2 : 1 std	0.008918	0.008393	0.009519

We also test the CPU time of the algorithms by varying the system size while maintaining the particle density $N/L^3 = 0.01$. We measure the time cost per step and the results are shown in Fig. 3, where the number of particles takes from 6×10^5 to 4×10^7 by using 960 CPU cores. It can be observed that the simulation time of the IRBE has a linear scaling

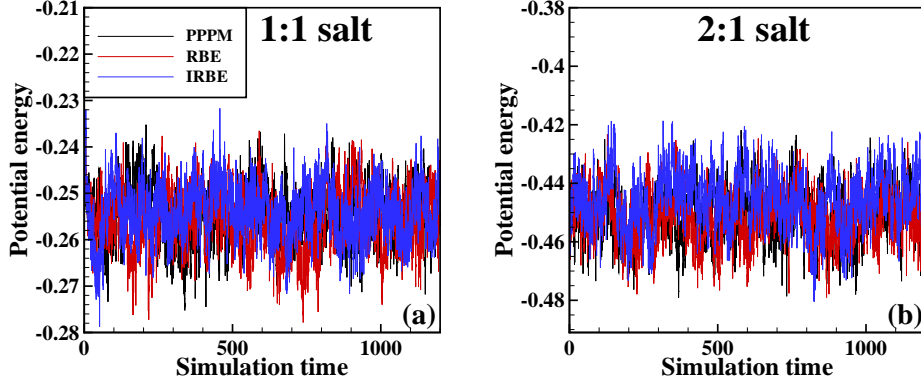


Figure 2: Potential energy per atom calculated by using the PPPM, RBE and the IRBE methods.

with the number of particles, and the computational efficiency by using the IRBE method is improved by a factor of 2 compared to the RBE, and a factor of 6 compared to the PPPM.

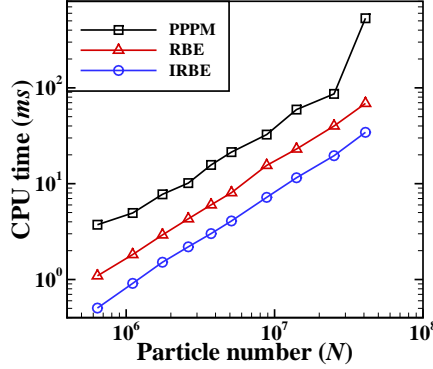


Figure 3: CPU time performance per timestep of the monovalent salt solution by using the PPPM, RBE and IRBE methods.

3.2 All-atom water systems

For the second benchmark problem, we conduct all-atom MD simulations of bulk water systems by using the SPC/E force field[53]. For validating the accuracy, a system consisting of 901 water molecules is used with simulation box of the side length $L = 3nm$. The Nosé-Hoover thermostat is applied with the coupling parameter $\gamma = 1.0$ and temperature $T = 298K$. In each simulation, we perform 5×10^5 time steps for equilibrium and another 6×10^5 steps for statistics. We choose the accuracy $1e-4$ in the PPPM method as reference. For the IRBE, we set parameters $(r_\eta, \tilde{p}) = (0.7nm, 100)$ for the short-range interactions, and $(\alpha, p) = (0.09, 200)$ for the long-range interactions. The setup balances the calculation time of these two parts and is near-optimal for time cost. Table. 2 list other groups of parameters which can achieve similar accuracy (with the error of RDF, MSD and energy is in $< 1\%$ error threshold) by our extensive simulations, which shall be useful to provide guidance for general all-atom simulations. All the different parameter sets given in Table. 2 can produce accurate simulation results due to that variance of the stochastic force is controlled, demonstrating the insensitivity of the IRBE to these parameters. With the increase of α , the force variance in Fourier space becomes larger and we need to increase p . At the same time, the error

complementary function decreases, so one can choose smaller (r_η, \tilde{p}) . These parameters are determined empirically and are difficult to be given theoretically. Some valuable criteria may be related to the practical choice of parameters, e.g., the symmetry-preserving mean-field condition presented recently[54]. We will report further demonstrations of these criteria in our subsequent work. Fig. 4 presents the RDFs and MSDs produced by different methods between oxygen atoms. These data vadiate the accuracy of the IRBE method as it well reproduces the result of the other two methods.

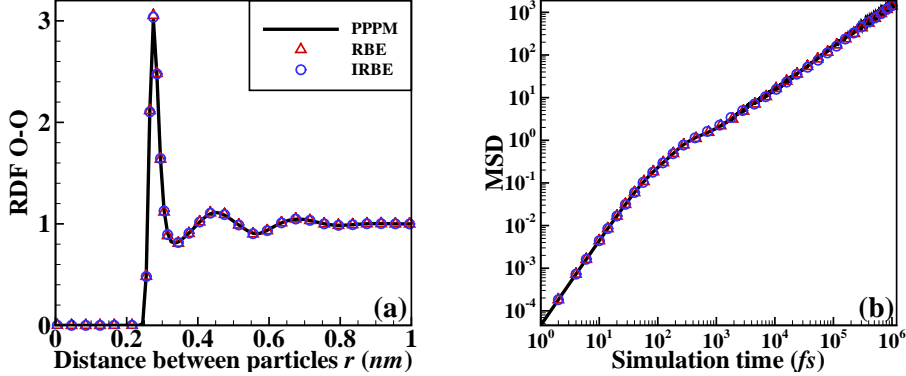


Figure 4: RDFs and MSDs calculated by using the PPPM, RBE and IRBE methods for the bulk water system.

Table 2: The choice of parameters in the IRBE method for the bulk water system, where the result of RDF, MSD and energy is in $< 1\%$ error threshold. (Unit of length: nm)

Fourier space		Real space ($r_c = 1.2nm$)
α	p	(r_η, \tilde{p})
0.10	300	(0.6, 100) and (0.7, 50)
0.09	200	(0.6, 150) and (0.7, 100)
0.08	200	(0.6, 200) and (0.7, 100)
0.07	200	(0.6, 300) and (0.7, 200)
0.06	100	(0.6, 400) and (0.7, 300)
0.05	100	(0.6, 500) and (0.7, 400)

Finally, we study the CPU performance with the same algorithm parameters by taking a large size of water systems with 10^8 water molecules and varying the number of CPU cores from 1000 to 50000. The results are shown in Fig. 5. The CPU time per step of the IRBE method has linearly decrease with respect to the number of CPU cores, while the parallel efficiency of the PPPM method decrease when the core number exceeds 10000. The decrease of the scalability of the PPPM can be understood as the increase of cost in CPU communication. In comparison to the RBE, the IRBE method further improves the computational efficiency due to the acceleration in calculating short-range interactions.

4 Conclusions

In summary, we develop an improved version of the RBE method for non-bonded interactions in MD simulations, which accurately and efficiently reproduces the structure and dynamical information of the RBE and the PPPM method for benchmark problems. The

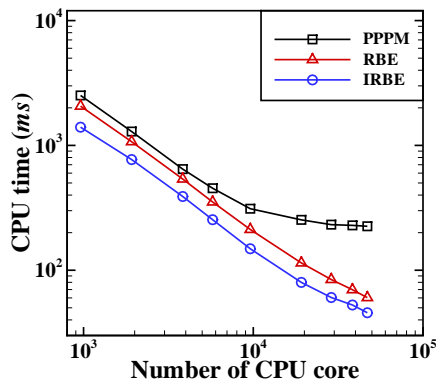


Figure 5: CPU cost per step of the bulk water system by using the PPPM, RBE and IRBE methods.

IRBE method is a stochastic approximation to the non-bonded forces, which benefits from random mini-batch strategy in both the Fourier space for the long-range interactions and the real-space cutoff for the short-range interactions, leading to efficient and memory-saving algorithm, achieving an optimal $\mathcal{O}(N)$ scaling. Analysis on the stability and convergency are also provided. The simulations on primitive-model electrolyte and all-atom bulk water systems are conducted to demonstrate the accuracy and attractive performance of the IRBE algorithm.

The IRBE method is implemented in parallel programming with the MPI and OpenMP. It will be also great significance for broader use of the algorithm if there is a version with the graphic processing units, and we are working on it currently. Moreover, extension of the method to quasi-2D systems with planar interfaces, in particular with the dielectric mismatch [55, 26, 56] is straightforward and shall be studied in our subsequent work. The IRBE method is expected to play an important role for simulating problems in applications at chemical physics, materials and biological systems.

Acknowledgements

The authors acknowledge the financial support from the National Natural Science Foundation of China (grant No. 12071288), Science and Technology Commission of Shanghai Municipality (grant Nos. 20JC1414100 and 21JC1403700), and the support from the HPC center of Shanghai Jiao Tong University.

Conflict of interest

The authors declare that they have no conflict of interest.

Data Availability Statement

The data that support the findings of this study are available from the corresponding author upon reasonable request.

References

- [1] M. Karplus, G. A. Petsko, Molecular dynamics simulations in biology, *Nature* 347 (6294) (1990) 631–639.

- [2] S. A. Hollingsworth, R. O. Dror, Molecular dynamics simulation for all, *Neuron* 99 (6) (2018) 1129–1143.
- [3] V. Yamakov, D. Wolf, S. R. Phillpot, A. K. Mukherjee, H. Gleiter, Dislocation processes in the deformation of nanocrystalline aluminium by molecular-dynamics simulation, *Nat. Mat.* 1 (1) (2002) 45–49.
- [4] A. T. Brünger, J. Kuriyan, M. Karplus, Crystallographic R factor refinement by molecular dynamics, *Science* 235 (4787) (1987) 458–460.
- [5] M. P. Allen, D. J. Tildesley, *Computer Simulation of Liquids*, Oxford University Press, 2017.
- [6] B. R. Brooks, R. E. Bruccoleri, B. D. Olafson, D. J. States, S. a. Swaminathan, M. Karplus, CHARMM: A program for macromolecular energy, minimization, and dynamics calculations, *J. Comput. Chem.* 4 (2) (1983) 187–217.
- [7] Y. Burak, G. Ariel, D. Andelman, Onset of DNA aggregation in presence of monovalent and multivalent counterions, *Biophys. J.* 85 (4) (2003) 2100–2110.
- [8] C. M. Davis, R. B. Dyer, The role of electrostatic interactions in folding of β -proteins, *J. Am. Chem. Soc.* 138 (4) (2016) 1456–1464.
- [9] H.-X. Zhou, X. Pang, Electrostatic interactions in protein structure, folding, binding, and condensation, *Chem. Rev.* 118 (4) (2018) 1691–1741.
- [10] C. Ghosh, B. Jana, Curious case of MAD2 protein: Diverse folding intermediates leading to alternate native states, *J. Phys. Chem. B* 126 (9) (2022) 1904–1916.
- [11] C. Schiel, M. Vogtland, R. Bechstein, A. Kußnle, P. Maass, Molecular stripe patterns on surfaces in the presence of long-range repulsive electrostatic interactions: Monte Carlo simulations and mean-field theory, *J. Phys. Chem. C* 125 (37) (2021) 20650–20657.
- [12] E. N. Frigini, R. D. Porasso, Effect of ionic strength on ibuprofenate adsorption on a lipid bilayer of dipalmitoylphosphatidylcholine from molecular dynamics simulations, *J. Phys. Chem. B* 126 (9) (2022) 1941–1950.
- [13] M. Lund, B. Jönsson, Charge regulation in biomolecular solution, *Q. Rev. Biophys.* 46 (3) (2013) 265–281.
- [14] D. Frenkel, B. Smit, *Understanding Molecular Simulation: From Algorithms to Applications*, 2nd Edition, Elsevier, 2010.
- [15] L. Verlet, Computer “experiments” on classical fluids. I. Thermodynamical properties of Lennard-Jones molecules, *Phys. Rev.* 159 (1) (1967) 98.
- [16] B. Quentrec, C. Brot, New method for searching for neighbors in molecular dynamics computations, *J. Comput. Phys.* 13 (3) (1973) 430–432.
- [17] A. P. Thompson, H. M. Aktulga, R. Berger, D. S. Bolintineanu, W. M. Brown, P. S. Crozier, P. J. in’t Veld, A. Kohlmeyer, S. G. Moore, T. D. Nguyen, et al., LAMMPS-A flexible simulation tool for particle-based materials modeling at the atomic, meso, and continuum scales, *Comput. Phys. Commun.* 271 (2021) 108171.
- [18] M. J. Abraham, T. Murtola, R. Schulz, S. Páll, J. C. Smith, B. Hess, E. Lindahl, GROMACS: High performance molecular simulations through multi-level parallelism from laptops to supercomputers, *SoftwareX* 1 (2015) 19–25.
- [19] T. A. Darden, D. M. York, L. G. Pedersen, Particle mesh Ewald: an $N\log(N)$ method for Ewald sums in large systems, *J. Chem. Phys.* 98 (12) (1993) 10089–10092.

- [20] R. W. Hockney, J. W. Eastwood, *Computer Simulation Using Particles*, Taylor & Francis, 1988.
- [21] U. Essmann, L. Perera, M. L. Berkowitz, T. Darden, H. Lee, L. Pedersen, A smooth particle mesh Ewald method, *J. Chem. Phys.* 103 (19) (1995) 8577–8593.
- [22] J. Barnes, P. Hut, A hierarchical $O(N \log N)$ force-calculation algorithm, *Nature* 324 (6096) (1986) 446–449.
- [23] L. Greengard, Fast algorithms for classical physics, *Science* 265 (5174) (1994) 909–914.
- [24] A. C. Maggs, V. Rossetto, Local simulation algorithms for Coulomb interactions, *Phys. Rev. Lett.* 88 (19) (2002) 196402.
- [25] B. Kohnke, C. Kutzner, H. Grubmüller, A GPU-accelerated Fast Multipole Method for GROMACS: Performance and accuracy, *J. Chem. Theory Comput.* 16 (11) (2020) 6938–6949.
- [26] J. Liang, J. Yuan, Z. Xu, HSMA: An $O(N)$ electrostatics package implemented in LAMMPS, *Comput. Phys. Commun.* (2022) 108332.
- [27] S. Plimpton, Fast parallel algorithms for short-range molecular dynamics, *J. Comput. Phys.* 117 (1) (1995) 1–19.
- [28] C. Begau, G. Sutmann, Adaptive dynamic load-balancing with irregular domain decomposition for particle simulations, *Comput. Phys. Commun.* 190 (2015) 51–61.
- [29] A. Arnold, F. Fahrenberger, C. Holm, O. Lenz, M. Bolten, H. Dachsel, R. Halver, I. Kabadshow, F. Geller, F. Heber, Comparison of scalable fast methods for long-range interactions, *Phys. Rev. E* 88 (6) (2013) 063308.
- [30] D. A. Walker, B. Kowalczyk, M. O. de la Cruz, B. A. Grzybowski, Electrostatics at the nanoscale, *Nanoscale* 3 (4) (2011) 1316–1344.
- [31] R. H. French, V. A. Parsegian, R. Podgornik, R. F. Rajter, A. Jagota, J. Luo, D. Asthagiri, M. K. Chaudhury, Y.-m. Chiang, S. Granick, Long range interactions in nanoscale science, *Rev. Mod. Phys.* 82 (2) (2010) 1887.
- [32] C. E. Leiserson, N. C. Thompson, J. S. Emer, B. C. Kuszmaul, B. W. Lampson, D. Sanchez, T. B. Schardl, There’s plenty of room at the Top: What will drive computer performance after Moore’s law?, *Science* 368 (6495) (2020) eaam9744.
- [33] Y. Sherry, N. C. Thompson, How Fast Do Algorithms Improve?, *Proc. IEEE Inst. Electr. Electron. Eng.* 109 (11) (2021) 1768–1777.
- [34] S. S. Kortum, Research, patenting, and technological change, *Econometrica* (1997) 1389–1419.
- [35] C. Predescu, A. K. Lerer, R. A. Lippert, B. Towles, J. Grossman, R. M. Dirks, D. E. Shaw, The U-series: A separable decomposition for electrostatics computation with improved accuracy, *J. Chem. Phys.* 152 (8) (2020) 084113.
- [36] J. Liang, P. Tan, Y. Zhao, L. Li, S. Jin, L. Hong, Z. Xu, Superscalability of the random batch Ewald method, *J. Chem. Phys.* 156 (1) (2022) 014114.
- [37] D. Lu, H. Wang, M. Chen, L. Lin, R. Car, E. Weinan, W. Jia, L. Zhang, 86 PFLOPS deep potential molecular dynamics simulation of 100 million atoms with ab initio accuracy, *Comput. Phys. Commun.* 259 (2021) 107624.
- [38] S. Jin, L. Li, Z. Xu, Y. Zhao, A random batch Ewald method for particle systems with Coulomb interactions, *SIAM J. Sci. Comput.* 43 (4) (2021) B937–B960.

- [39] J. Liang, P. Tan, L. Hong, S. Jin, Z. Xu, L. Li, A random batch Ewald method for charged particles in the isothermal-isobaric ensemble, arXiv preprint arXiv:2110.14362.
- [40] J. Liang, Z. Xu, Y. Zhao, Random-batch list algorithm for short-range molecular dynamics simulations, *J. Chem. Phys.* 155 (4) (2021) 044108.
- [41] S. Jin, L. Li, J.-G. Liu, Random Batch Methods (RBM) for interacting particle systems, *J. Comput. Phys.* 400 (2020) 108877.
- [42] P. P. Ewald, Die Berechnung optischer und elektrostatischer Gitterpotentiale, *Ann. Phys.-Berlin* 369 (3) (1921) 253–287.
- [43] J. Kolafa, J. W. Perram, Cutoff errors in the Ewald summation formulae for point charge systems, *Mol. Simulat.* 9 (5) (1992) 351–368.
- [44] Z. Yao, J.-S. Wang, G.-R. Liu, M. Cheng, Improved neighbor list algorithm in molecular simulations using cell decomposition and data sorting method, *Comput. Phys. Commun.* 161 (1-2) (2004) 27–35.
- [45] U. Welling, G. Germano, Efficiency of linked cell algorithms, *Comput. Phys. Commun.* 182 (3) (2011) 611–615.
- [46] S. Páll, B. Hess, A flexible algorithm for calculating pair interactions on SIMD architectures, *Comput. Phys. Commun.* 184 (12) (2013) 2641–2650.
- [47] M. P. Howard, J. A. Anderson, A. Nikoubashman, S. C. Glotzer, A. Z. Panagiotopoulos, Efficient neighbor list calculation for molecular simulation of colloidal systems using graphics processing units, *Comput. Phys. Commun.* 203 (2016) 45–52.
- [48] N. Tchipev, S. Seckler, M. Heinen, J. Vrabec, F. Gratl, M. Horsch, M. Bernreuther, C. W. Glass, C. Niethammer, N. Hammer, et al., TweTriS: Twenty trillion-atom simulation, *Int. J. High Perform. Comput. Appl.* 33 (5) (2019) 838–854.
- [49] S. J. Pennycook, C. J. Hughes, M. Smelyanskiy, S. A. Jarvis, Exploring SIMD for molecular dynamics, using Intel® Xeon® processors and Intel® Xeon Phi coprocessors, in: 2013 IEEE 27th International Symposium on Parallel and Distributed Processing, IEEE, 2013, pp. 1085–1097.
- [50] M. Deserno, C. Holm, How to mesh up Ewald sums. II. An accurate error estimate for the particle–particle–particle–mesh algorithm, *J. Chem. Phys.* 109 (18) (1998) 7694–7701.
- [51] P. J. in’t Veld, S. J. Plimpton, G. S. Grest, Accurate and efficient methods for modeling colloidal mixtures in an explicit solvent using molecular dynamics, *Comput. Phys. Commun.* 179 (5) (2008) 320–329.
- [52] R. W. Hockney, J. W. Eastwood, *Computer Simulation Using Particles*, CRC Press, 2021.
- [53] P. Mark, L. Nilsson, Structure and dynamics of the TIP3P, SPC, and SPC/E water models at 298 K, *J. Phys. Chem. A* 105 (43) (2001) 9954–9960.
- [54] Z. Hu, The symmetry-preserving mean field condition for electrostatic correlations in bulk, *J. Chem. Phys.* 156 (3) (2022) 034111.
- [55] J. Liang, J. Yuan, E. Luijten, Z. Xu, Harmonic surface mapping algorithm for molecular dynamics simulations of particle systems with planar dielectric interfaces, *J. Chem. Phys.* 152 (13) (2020) 134109.
- [56] J. Yuan, H. S. Antila, E. Luijten, Particle–particle particle–mesh algorithm for electrolytes between charged dielectric interfaces, *J. Chem. Phys.* 154 (9) (2021) 094115.